Defence Science Journal, Vol. 72, No. 2, March 2022, pp. 205-216, DOI : 10.14429/dsj.72.17232

Evaluation of Steel and Tungsten Carbide – Cobalt (WC-8Co) 5.56 × 45 mm Calibre Projectile Penetration into Silicon Carbide (SiC): Experiment and Numerical Simulation

Abdul Basyir,[#,*] Romie Oktovianus Bura,[$] Denny Lesmana,[%] and Lucia Dwi Antika[^]

[#]*Research Center for Physics, National Research and Innovation Agency, Banten – 15314, Indonesia*
[$]*Faculty of Defense Technology, Indonesia Defense University, West Java – 16810, Indonesia*
[%]*Ammunition Division, PT. Pindad (Persero), East Java – 65175, Indonesia*
[^]*Research Center for Chemistry, National Research and Innovation Agency, Banten – 15314, Indonesia*
[*]*E-mail: abdulbasyir037@gmail.com*

ABSTRACT

This study aims to evaluate WC-8Co as a substitution material in a standard steel core projectile commercially produced by PT Pindad (Persero). The enhanced performance of 5.56 x 45-millimeter ammunition after the addition of WC-8Co hard metal was evaluated in terms of penetration into a silicon carbide (SiC) target. Numerical simulations and analysis of the ballistic impact of WC-8Co on ceramic targets were verified by experimental data. The results show that front core substitution in SS109 bullets from steel (Pindad standard) to WC-8Co resulted in 1.5 times greater DoP. Although projectiles with steel (Pindad standard) as the front core have a muzzle velocity higher than those using WC-8Co, they have a lower kinetic energy than the latter. In addition, WC-8Co cemented carbides also displayed higher crater and residual velocity on SiC targets; around 1.8 and 1.3 times higher, respectively. These findings demonstrate the potential use of WC-8Co for development as front core material to improve the penetration of projectiles into ceramic armour.

Keywords: WC-8Co, steel (Pindad standard), ballistic impact, SiC

1. INTRODUCTION

Ceramic materials have been widely used in recent years in armour applications due to their properties, having a relatively low density, a high level of hardness, and great compressive strength[1]. These ceramic characteristics play a principal role in increasing ballistic performance, since they potentially crush the projectiles, thus leading to inefficiency in projectile penetration[2]. Despite their advantages, ceramics demonstrate low tensile strength and high sensitivity toward mechanical defects. Therefore, many studies have been conducted to improve ceramic strength and lower its susceptibility to failure to improve the quality of ceramic armour technology. Several ceramic materials, including Silicon Carbide (SiC), Silicon Nitride (Si_3N_4), Aluminum Oxide (Al_2O_3), and Boron Carbide (B_4C), are widely used in armour applications and have been employed by the US military. Among these, B_4C is considered the best ceramic armour since it is lighter and harder, but unfortunately more expensive than other materials[3]. SiC, on the other hand, possesses reasonable ballistic performance[4-5] at an affordable price[6]. Currently, SiC with 99.2 per cent of purity is employed as a material in armour technology.

Improving the penetration effect of ammunition is often associated with the choice of material used in the projectile core. Tungsten-based materials are those mainly used as core materials in projectiles to change steel material. Some research on tungsten-based penetrators of silicon carbide has already been conducted, such as that of Holmquist, Johnson, and Gooch[7], who used WC-6Co as a core material in ARL BS41 14.5 mm calibre projectiles. WC-6Co was located in the back position of this position, surrounded by lead and steel. Lundberg and Lundberg[8] used tungsten alloy with a diameter and length of 2 mm and 80 mm as a penetrator, while Behner, Heine, and Wickert[9] used tungsten heavy alloy (WHA) (W-Ni-Fe) with a length of 90 mm and a diameter of 6 mm, and Luo *et al.*[10] a length of 40 mm and diameter of 16 mm. Yuan, Tan, and Goh[11] used pure tungsten with a length and diameter of 60 mm and 5 mm as a long rod penetrator. All these penetrators can perforate SiC targets because material based on tungsten has a superior density and is very hard. For the same penetrator dimensions and design, these properties play a major role in creating a deep depth of penetration (DoP)[4].

However, amongst these various tungsten-based penetrators, the penetration effect of WC-8Co on SiC targets has yet to be established, especially for an actual small caliber. Therefore, this research uses the standard 5.56 × 45 mm NATO projectile design, which is one of the most common types of bullets used and demanded by the military. In addition, the NATO 5.56 x 45 mm bullet calibre has been employed by

Received : 02 August 2021, Revised : 20 January 2022
Accepted : 11 February 2022, Online published : 11 May 2022

the PT. Pindad (Persero) factory in locally-produced weapon versions known as SS1 and SS2, standing for Assault Rifle-1 and -2 respectively. The original core of this projectile consists of lead and steel (Pindad standard).

To increase the penetration effect of such ammunition, material based on WC-Co was chosen to change the position of the steel (Pindad standard), as this is already known as a material with an excellent combination of mechanical and density (around 14 g/cm^3) properties[12-14]. Although its density is lower than WHA (between 17 to 19 g/cm^3)[15-17], its hardness (around is 1600 Hv) is higher than that of WHA, which is around 250 – 570 Hv[16-20], while the hardness of steel (Pindad standard) is around 600 Hv. There also exist tungsten intermetallic materials (XW_2) such as ZrW_2 and HfW_2, which also have great density and hardness, at around 14 g/cm^3 and 17 g/cm^3 [21] respectively. However, their hardness (around 700 and 970 Hv)[21-23] is lower than WC-Co-based material.

Furthermore, the mechanical property data demonstrate that WC-Co is approximately twice as hard as steel and with double the density[24]. In addition, WC-Co has a higher melting point and Young's modulus than steel, at 2870 °C and approximately 530-700 GPa respectively[25]. In this study, WC-8Co was chosen rather than WC-6Co because the enhanced Co percentage can increase the density, fracture toughness, and bending strength properties[26-28]. Therefore, the DoP produced by this material is expected to be optimum. Moreover, it is expected that the material could be potentially developed as a replacement for steel (Pindad standard) core projectiles.

This study was initiated to develop ammunition capability domestically within Indonesia. In it, the front core standard 5.56 x 45mm projectile ammunition was replaced by WC-8Co, which was designed to analyse the quantitative and qualitative damage performance parameters caused by a projectile on a target material. The performance of WC-8Co cemented carbides and steel (Pindad standard) as the front core of projectiles penetrating ceramic targets was comparatively analysed through experiments. Additionally, a numerical simulation model using ANSYS Explicit Dynamic software was developed to predict residual velocity and for further potential use as a reference for similar materials in terminal ballistics. No previous research has investigated the residual velocity effect of penetrators based on tungsten on SiC targets.

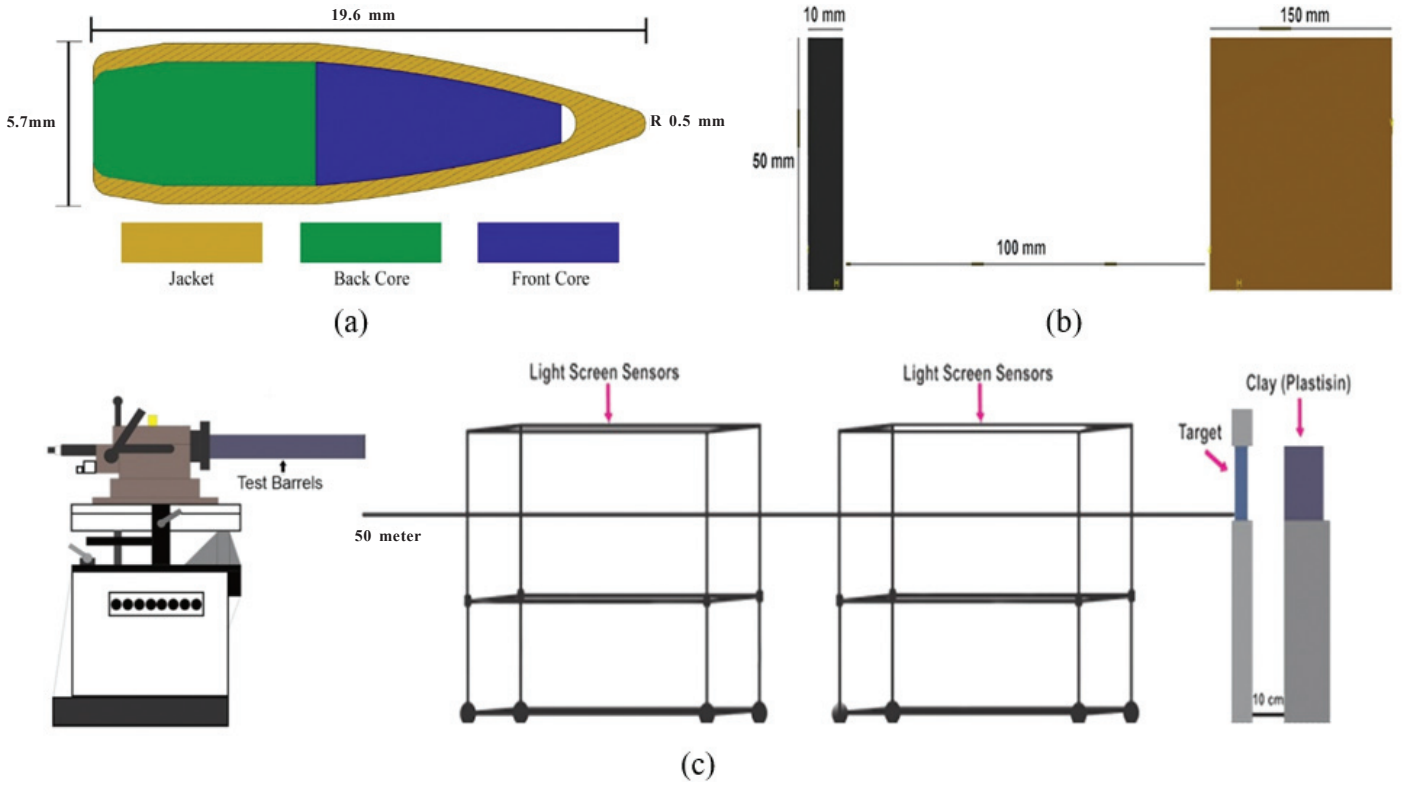

Figure 1. Design and schematic of: (a) the projectile, (b) the main - backing target, and (c) the ballistic test setup.

Table 1. Material specifications of the projectile parts

Projectile component	Mass (g)	Material type
Projectile back core	2 (± 0.1)	Lead antimony
Projectile front core 1	1.1 (±0.1)	WC – 8Co
Projectile front core 2	0.6 (±0.1)	Steel (Pindad standard)
Projectile jacket	1.3 (±0.1)	Brass (Cu (90%) - Zn (10%))

2. METHODOLOGY

2.1 Materials

5.56 × 45mm calibre ammunition, M855/SS109 NATO standard (STANAG 4172) and SS109 ammunition were provided by PT. Pindad (Persero). Other projectile components, such as propellant, primer, casing, projectile back core, and projectile ammunition jacket were equivalent to those employed in SS109 PT. Pindad (Persero) ammunition.

2.2 Projectile Structure

The projectile consisted of three parts: the back core, front core, and projectile jacket Fig. 1(a). Further, the material specification of these all parts are shown in Table 1.

2.3 Ballistic Measurements

The ballistic test was performed at PT. Pindad (Persero), in line with the Standard NATO Agreement (STANAG) 4241[29]. The ballistic perforation test was performed on an SiC target using 5.56 × 45 mm armour-piercing WC-8Co cored projectiles. The experimental setup was created according to the schemee, as shown in Figure 1(c). To evaluate the penetration of the projectile, WC-8Co and steel (Pindad standard) used as front core were tested. The main target was SiC with a thickness of 10 mm; the material employed in this research was equivalent to the ceramic material used for body armour application-levels III and IV[30], according to Qingdao Newthink New Materials Co. Ltd. an SiC manufacturing company. The thickness range of the ceramic layer used in body armour is around 7 mm - 10 mm[31].

The main targets were backed by ballistic plasticine/clay with a thickness of 150 mm, with a 100 mm air gap behind them Fig. 1(b). This distance was set to prevent damage to the backing target, due to the energy distribution from the fragmentation of projectile and target material. A large air gap was not used, as it can reduce the penetrating capability of projectiles[32].

The ballistic test experimental procedure consisted of three main steps: preparation, execution, and evaluation. For the preparation, the most suitable type of test barrel and sensor were selected, followed by determination of the firing distance between the gun barrel muzzle and target. For this study, the

Table 2. Technical WC – 6Co[7], tungsten (W) alloy[34], steel[35], lead and brass[36], and SiC[37] data

Parameter	Unit	WC-6Co	W Alloy	Steel	Lead	Brass	SiC
Density	$kg.m^{-3}$	14800	17680	7830	10660	8490	3160
Specific Heat	$J.kg^{-1}.K^{-1}$	250	134	477	124	385	0.000
Melting Temperature (Tm)	K	1768	1730	1793	760	1189	-
Reference Strain Rate	Sec^{-1}	1	1	1	0.0001	0.0005	-
Young's Modulus (E)	GPa	620	343	200	55	97	420
Poisson's Ratio (v)	-	0.215	0.28	0.290	0.42	0.310	0.160
Shear Modulus (G)	GPa	255	134	77	20	37	193
Bulk Modulus (K)	GPa	362		159	41	100	220
Johnson - Cook Strength (JCS) Mode							
Initial Yield Stress (A)	MPa	3000	1197	600	24	206	-
Hardening Coefficient (B)	MPa	89000	580	510	300	505	-
Hardening Exponent (n)	-	0.650	0.05	0.260	1	0.42	-
Strain Rate Coefficient (C)	-	0.000	0.025	0.014	0.1	0.01	-
Thermal Softening Exponent (m)	-	1.000	1.9	1.030	1	1.68	-
Johnson - Cook Failure (JCF) Mode							
Failure Model Constant (D1)	-	0.000	0.000	0.050	0.250	0.540	-
Failure Model Constant (D2)	-	0.002	0.002	3.440	0.000	4.890	-
Failure Model Constant (D3)	-	-3.000	-3.000	-2.120	0.000	3.030	-
Failure Model Constant (D4)	-	0.000	0.000	0.002	0.000	0.014	-
Failure Model Constant (D5)	-	0.000	0.000	0.610	0.000	1.120	-
Johnson - Holmquist Strength and Failure Mode							
Hugoniat Elastic Limit	MPa	-	-	-	-	-	11700
Intact Strength (A)	-	-	-	-	-	-	0.860
Intact Strength Exponent (n)	-	-	-	-	-	-	0.500
Strain Rate Constant (C)	-	-	-	-	-	-	0.009
Fracture Strength Constant (B)	-	-	-	-	-	-	0.400
Fracture Strength Exponent (m)	-	-	-	-	-	-	1.000
Maximum Fracture Strength Ratio (SFMAX)	-	-	-	-	-	-	0.132
Damage Constant (D1)	-	-	-	-	-	-	0.0612
Damage Constant (D2)	-	-	-	-	-	-	1.000
Bulking Constant (B)	-	-	-	-	-	-	1.000
Hydrodynamics Tensile Limit (T)	-	-	-	-	-	-	-750

distance between the gun muzzle and main target was set at 50 meters. The firing test was performed using three times for each different projectile type. The impact velocity, muzzle kinetic energy, and DoP value were measured after the test. Based on STANAG 4172, the muzzle kinetic energy of 5.56 × 45 mm ammunition is around 1500 J[33].

2.4 Numerical Simulation

The numerical simulation analysis was performed with the aid of the ANSYS Explicit Dynamic Interface. The simulation consisted of three main steps, which involved drawing the geometry of the projectile and target; inputting the projectile and target technical data, and analysing the numerical simulation model. The geometric figures were generated using CATIA™ V5 software. The technical data included the strength and failure modes for the projectile and target material, with reference to the Johnson-Cook and Johnson-Holmquist models respectively (Table 2). The parameters related to tungsten carbide-cobalt, steel, and silicon carbide were further investigated.

Furthermore, the complex geometries of the projectiles and target were created using tetrahedron and multi-zone meshing with the size of 0.8 – 1 mm, and the initial velocity for the simulation analysis was determined by the ballistic test results. The residual velocity, deformation form, and DoP value were evaluated.

3. RESULTS AND DISCUSSION

3.1 Numerical Simulation Result

The numerical simulation utilised a mesh size of 0.8-1.1 mm with the multizone and tetrahedron methods, involving 35,167 and 39,579 mesh elements for WC – 8Co and steel (Pindad standard) as the front core of the projectile respectively. DoP, RV, the volume of the residual projectile, and the impact phenomenon were obtained from the numerical simulation. The DoP results obtained were used as validators of the numerical simulation, and were further compared with the experimental DoP results from the ballistic test.

Based on the penetration in the numerical simulation, the DoP was calculated using equation (1). The DoP results relating to the penetration by WC-8Co and steel (Pindad standard) as the front core of the projectile can be seen in equations (2) and (3) respectively.

$$L_{DoP\_NS} = \frac{L_{BT\_NS}}{L_{BT\_P}} \times P_{DoP\_P} \quad (1)$$

$$L_{DoP\_NS} = \frac{150mm}{144.526mm} \times 33.274mm = 34.53mm \quad (2)$$

$$L_{DoP\_NS} = \frac{150mm}{154.432mm} \times 24.892mm = 24.18mm \quad (3)$$

Where

L_{DoP_NS} = DoP obtained from the numerical simulation

L_{BT_NS} = length of backing target from the numerical simulation

Table 3. Comparison between the DoP data from the experiment and numerical simulation of a projectile with a front core of WC – 8Co and steel (Pindad standard)

Projectile type (Front core)	DoP average (mm)	
	Experiment	Numerical simulation
WC – 8Co	36.65	34.53
Steel (Pindad standard)	24.24	24.18

Table 4. WC–8Co technical data for the numerical simulation

Parameter	Unit	Front Core of WC – 8Co
Density	$kg.m^{-3}$	14800
Specific Heat	$J.kg^{-1}.K^{-1}$	250
Melting Temperature (Tm)	K	1768
Reference Strain Rate	Sec^{-1}	1
Young Modulus (E)	GPa	620
Poisson's Ratio (v)	-	0.215
Shear Modulus (G)	GPa	255
Bulk Modulus (K)	GPa	362
Johnson - Cook Strength (JCS) Mode		
Initial Yield Stress (A)	MPa	1020
Hardening Coefficient (B)	MPa	867
Hardening Exponent (n)	-	0.440
Strain Rate Coefficient (C)	-	0.020
Thermal Softening Exponent (m)	-	1.750
Johnson - Cook Failure (JCF) Mode		
Failure Model Constant (D1)	-	0.030
Failure Model Constant (D2)	-	1.720
Failure Model Constant (D3)	-	-1.100
Failure Model Constant (D4)	-	0.000
Failure Model Constant (D5)	-	0.310
Damage Constant (D1)	-	-
Damage Constant (D2)	-	-
Bulking Constant (B)	-	-
Hydrodynamic Tensile Limit (T)	-	-

L_{DoP_P} = DoP obtained from the picture capture

L_{BT_P} = length of backing target from the picture capture

Table 3 shows a comparison of the DoP data from the numerical simulation and experimental results. It indicates that the simulation is very close to the experimental results, so can be utilised for further study.

The numerical simulation used technical data based on Table 2 for the steel (Pindad standard) as front core, lead as back core, brass as jacket, and SiC as target, but not for the WC-8Co as front core. The WC-6Co and W alloy data presented in Table 2 were not suitable for producing a DoP

similar to that of the experimental test for the penetration of WC-8Co as front core projectile. Therefore, the technical data in Table 2 were optimised for the WC-8Co; these optimisation results can be seen in Table 4. The data were optimised using the iteration process. Because the point of interest of the numerical simulation was the residual velocity parameter. In which this parameter has a linear relation with impact energy[38-39], which itself has a linear relation with DoP[24]. Therefore, to obtain the best value of this parameter, the DoP generated from the numerical simulation must be close to the DoP value from the ballistic test. The simulation used the basic properties of WC-8Co from its experimental data. In addition, the values of the JCS and JCF mode for WC-8Co used modified values of JCS and JCF from steel by Johnson and Cook[35], because in this numerical simulation the JCS and JCF values for steel can generate a DoP that is similar to that of the experiment, which was produced by a projectile with a steel (Pindad standard) core. Theoretically, the strength values have a linear relation with the DoP, while the failure values are inversely proportional to the DoP. Therefore, JCS and JCF values from steel were multiplied and divided by the DoP ratio from the ballistic test.

3.2 Residual Velocity Effect on DoP at the Backing Target

Two projectile types were used for the study, with the difference between them only being the material type at the front of the projectile core. WC-8Co was employed for the front core of projectile A, while in projectile B steel (Pindad standard) was used. WC-8Co possesses a superior density (14.80 g/cm^3) and hardness (1675.29 Hv) to steel (Pindad standard), with the density and hardness of steel (Pindad standard) being 7.83 g/cm^3 and 656.43 Hv. In addition, the target SiC material has the highest hardness, at arond 2550 Hv. On the other hand, WC-8Co demonstrated the highest density, followed by steel (Pindad standard) and SiC[40].

The density of WC-8Co is 1.89 times higher than that of steel (Pindad standard). Consequently, although the volume size of the front core of both projectiles was the same, their masses were different. Therefore, the mass of the WC-8Co core projectile was 1.125 times higher than that with a steel (Pindad standard), at 4.5 and 4.0 grams respectively. Since the kinetic energy equation shows the linear correlation between mass and kinetic energy, higher mass results in higher energy kinetic, and vice versa. Even though a higher mass can reduce the projectile velocity, in this case the velocity gap has no great effect on the kinetic energy produced. Therefore, the projectile with WC-8Co as the front core still had greater kinetic energy than that with steel (Pindad standard). Indirectly, the higher mass projectile will thus also generate a greater DoP. The experimental data show that the kinetic energy has a linear relation with the DoP, with a high kinetic energy generating a greater DoP, and vice versa. In the experiment, the WC-8Co and steel (Pindad standard) core projectiles produced an average kinetic energy of 1733.57 joules and 1576.20 joules respectively, and an average DoP of 39.45 mm and 21.88 mm. Based on the data, the projectile with a front core of WC-8Co generated a DoP 1.5 times greater than the steel (Pindad standard) projectile, in terms of the main SiC target.

Figure 2 shows that based on the numerical simulation, the residual velocity for the WC-8Co projectile jacket was lower than that of the steel (Pindad standard) core projectile,

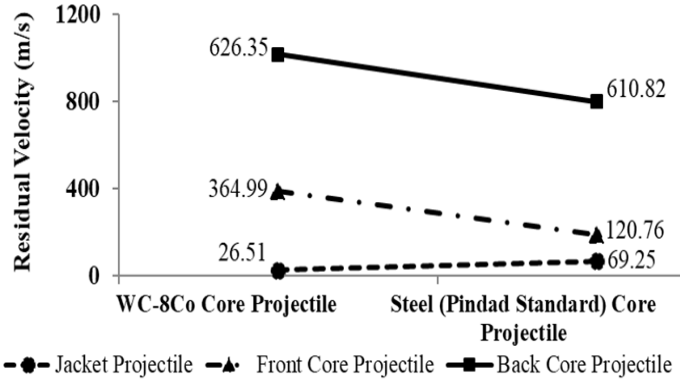

Figure 2. Residual velocity (RV) from the numerical simulation method for each component from projectile with front core of WC – 8Co and steel (Pindad standard).

Table 5. DoP and crater diameter data of WC-8Co and steel (Pindad standard) front core projectiles on penetration of the backing target, plasticine clay

Projectile type	Sample number	DoP of plasticine (150 mm)				Diameter (mm)		
		1	2	3	Average	x	y	Average
WC – 8Co	1	35.14	35.96	37.01	36.04	38.10	40.77	39.44
	2	35.39	35.54	37.24	36.06	41.43	43.39	42.41
	3	37.31	37.86	38.41	37.86	35.23	37.76	36.50
	Average	35.95	36.45	37.55	36.65	38.25	40.64	39.45
Steel (Pindad standard)	1	28.72	29.01	29.23	28.99	30.61	32.14	31.38
	2	24.08	24.62	24.71	24.47	18.29	20.07	19.18
	3	18.11	19.05	20.64	19.27	14.83	15.32	15.08
	Average	23.64	24.23	24.86	24.24	21.24	22.51	21.88

while the residual velocity of the front and back core of the WC-8Co projectile was higher than the corresponding steel (Pindad standard) projectile. The average residual velocity of the WC-8Co and steel (Pindad standard) core projectiles was 339.28 and 266.94 m/s respectively. These findings indicate that the penetration of the projectile with a front core of WC-8Co generated a residual velocity 1.3 times higher than that of the projectile with a steel front core.

The extent of the residual velocity is influenced by the level of impact kinetic energy, with a higher energy generating a higher residual velocity. Moreover, the residual velocity affects the size of the DoP results; a higher residual velocity generates a higher DoP, and vice versa. This can be explained by the fact that after the projectile has perforated the target, one with a higher residual velocity can penetrate deeper than one with a lower residual velocity. In addition, the difference in the level of residual velocity in each projectile component (jacket, front core, and back core) is dependent on the hardness of the material of each projectile component. More details of this will be given in the following section.

3.3 Hardness Effect on the Diameter Crater at Backing Target

From three firings, the WC-8Co and steel (Pindad standard) core projectiles generated average crater diameters of 39.45 mm and 21.88 mm respectively (Table 5). Based on these data, the projectile with a front core of WC-8Co created a crater diameter 1.8 times larger than that with a steel (Pindad standard) front core. This was caused by the quantity of residual projectile, with the numerical simulation results showing that the residual from the WC-8Co core projectile was greater than that of the steel (Pindad standard) core projectile (Fig. 3). Figure 3 also illustrates that after perforation of the SiC target, the WC-8Co core projectile had a front core residual greater than that of the steel (Pindad standard) equivalent. Additionally, the volume of the residual jacket of both projectiles was smaller than that of the front and back core. This possibly occurred as the jacket was the first projectile component to hit the target material in the penetration process. Moreover, the hardness of the jacket is considerably lower than that of the other components, at around 52 BHN[41]. The residual back core of both projectiles demonstrates the highest residual velocity, since it was the last component to hit the target material (SiC). In addition, the loss mass of the jacket and front core after perforation of the SiC was converted into energy.

In addition, based on Figure 3, after both projectiles had perforated the SiC target, that with the front core of WC-8Co generated a smaller volume of residual jacket than that with a front core of steel (Pindad standard), with most of WC-8Co jacket left on the surface of the backing target. This can be explained by the fact that the experiment data demonstrate that a large quantity of jacket projectile was found on the surface of the backing material from the perforation by the WC-8Co core projectile, while only a small quantity was found after

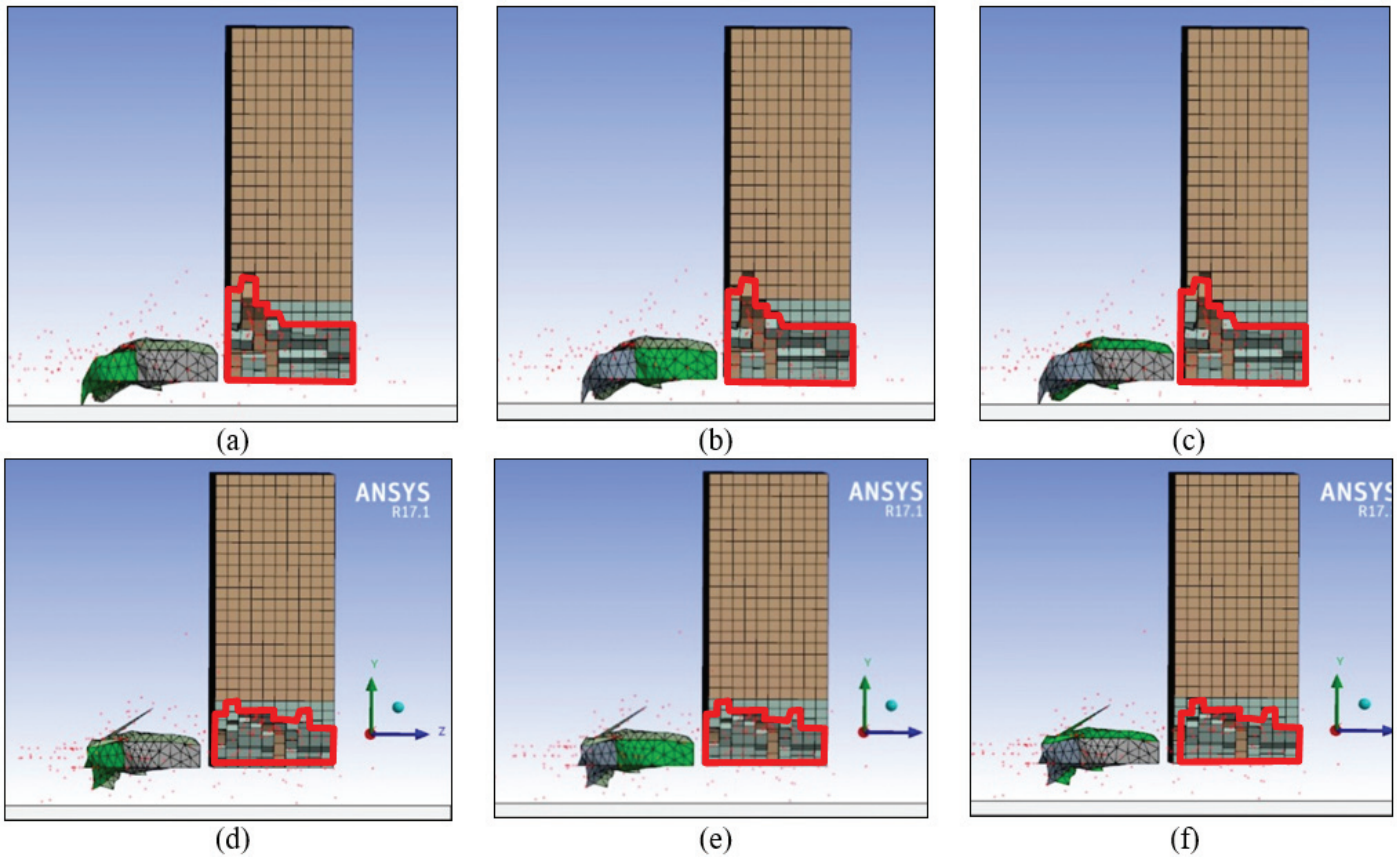

Figure 3. Residual projectile from the front core (a, d); the back core (b, e); and (c, f) the jacket for the projectile with a front core of WC-8Co (a-c) and steel (Pindad standard) (d-f).

the perforation of the steel (Pindad standard) core projectile (Fig. 4). This was because WC-8Co is harder than steel (Pindad standard). When the jacket of the front core of the WC-8Co projectile hit the SiC surface, it experienced significant erosion in two directions, from the front (SiC) and back (WC-8Co) of the jacket projectile. As a result, the jacket was highly eroded and left a mess on the surface of the backing target. It was different when the jacket of the front core of steel (Pindad standard) hit the SiC surface, as it experienced notable erosion in one direction only, from the SiC at the front of the jacket projectile. Therefore, the projectile jacket did not greatly erode, and was only broken up into multiple smaller fragments during the perforation process. These findings are also supported by the research of Behner *et al.*[9], in that the particular erosion that occurred on the projectile was caused by the ceramic target, even though the target did not have a lateral stockade.

Figure 5 shows the crater on the backing target, indicating that the penetration of the projectile with front core of WC-8Co generated a circular crater. In contrast, the penetration of the projectile with a front core of steel (Pindad standard) produced an irregular crater with small holes on the surface of the backing target. These holes were probably caused by penetration of small fragments from a projectile component, such as the projectile jacket. Since this has insignificant hardness, the resulting fragment size is relatively small.

The size of the residual projectile was influenced by the hardness of the front core of the projectile. During the perforation process of the WC-8Co front core of the SiC main target, the projectile was eroded due to its hardness. In addition, SiC is harder than both projectiles; Crouch[42] and Bracamonte *et al.*[43] state that the hardness of the main target material plays a role in enhanced ballistic resistance. However, since the projectile material is also very hard and strong, the major erosion and deformation effect on the SiC could be minimised.

Moreover, as the front core, WC-8Co can protect the back core better than steel (Pindad standard). As result, the back core of the projectile with WC-8Co produced a higher residual velocity than the steel equivalent. The impact velocity of the

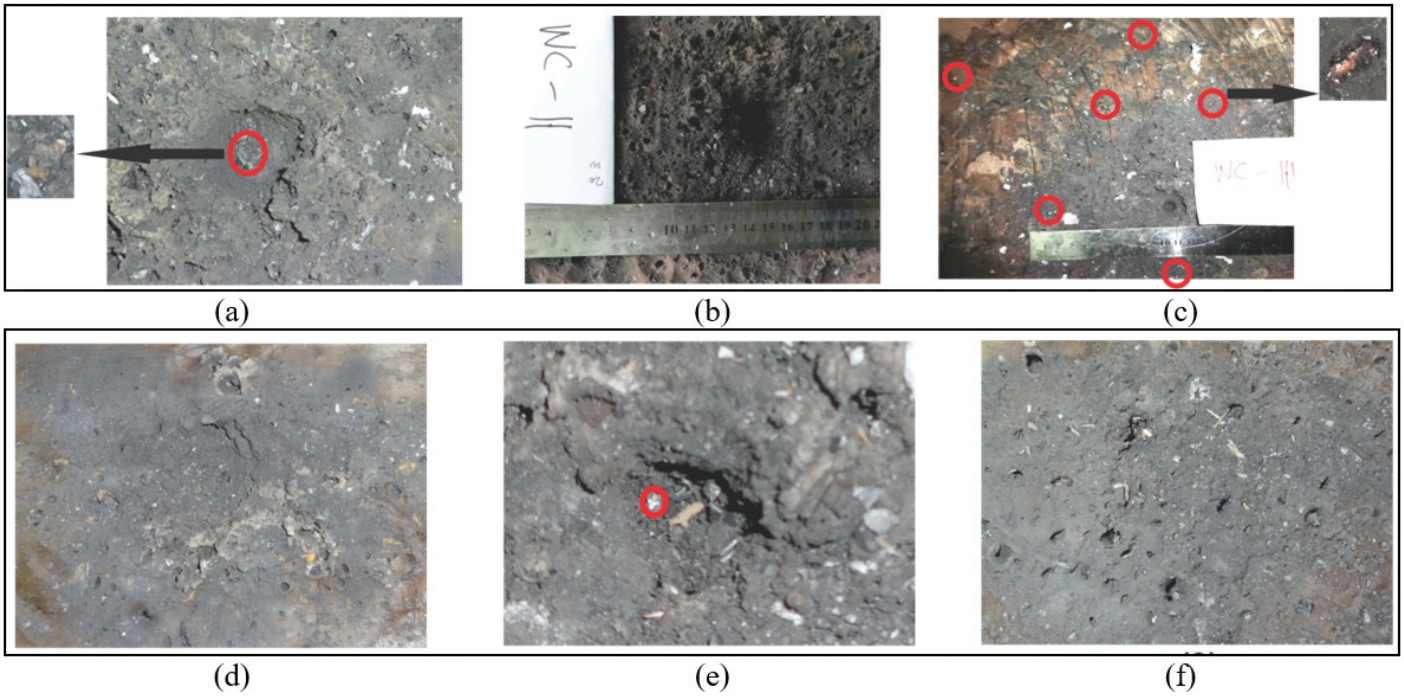

Figure 4. Fragment of the residual projectile (red circle) from WC-8Co (a-c) and steel (Pindad standard) (d-f) as the front core of the projectile on the surface of the backing target.

projectile with a steel front core was higher than that of WC-8Co; on the contrary, the WC-8Co residual velocity was higher than the projectile with front core of steel (Pindad standard). This shows that the hardness of WC-8Co plays an important role (besides the impact of kinetic energy) in minimising the erosion effect of SiC as the target material.

In addition, after perforating the SiC target, the projectile with the front core of WC-8Co experienced lower stress than that with a steel (Pindad standard) front core (Fig. 6a and Fig. 6c). The highest strain on the steel projectile was 688.51 MPa. As the value of yield stress of this steel is 600 MPa, the stress experienced by the projectile was over the elastic area, so this projectile got permanent deformation. On the other hand, the projectile with WC-8Co as the front core had the highest stress of 1118 MPa, which is lower than the yield stress of WC-8Co, with the initial yield of WC-8Co in the simulation being 1020 MPa.

From the strain data, it can be seen that the projectile jacket and rest of the front core area of the projectile using steel (Pindad standard) experienced the highest strain, while its back core only experienced minor strain as it was covered by the steel (Pindad standard) used in the front core. Such plastic strain takes place in almost all areas of this projectile. On the other hand, for the projectile with the WC-8Co front core, the greatest strain was experienced in at the front of the front core and in the area between the front and back cores. However, the plastic strain on this projectile was smaller than on the steel projectile (Fig. 6b and Fig. 6d).

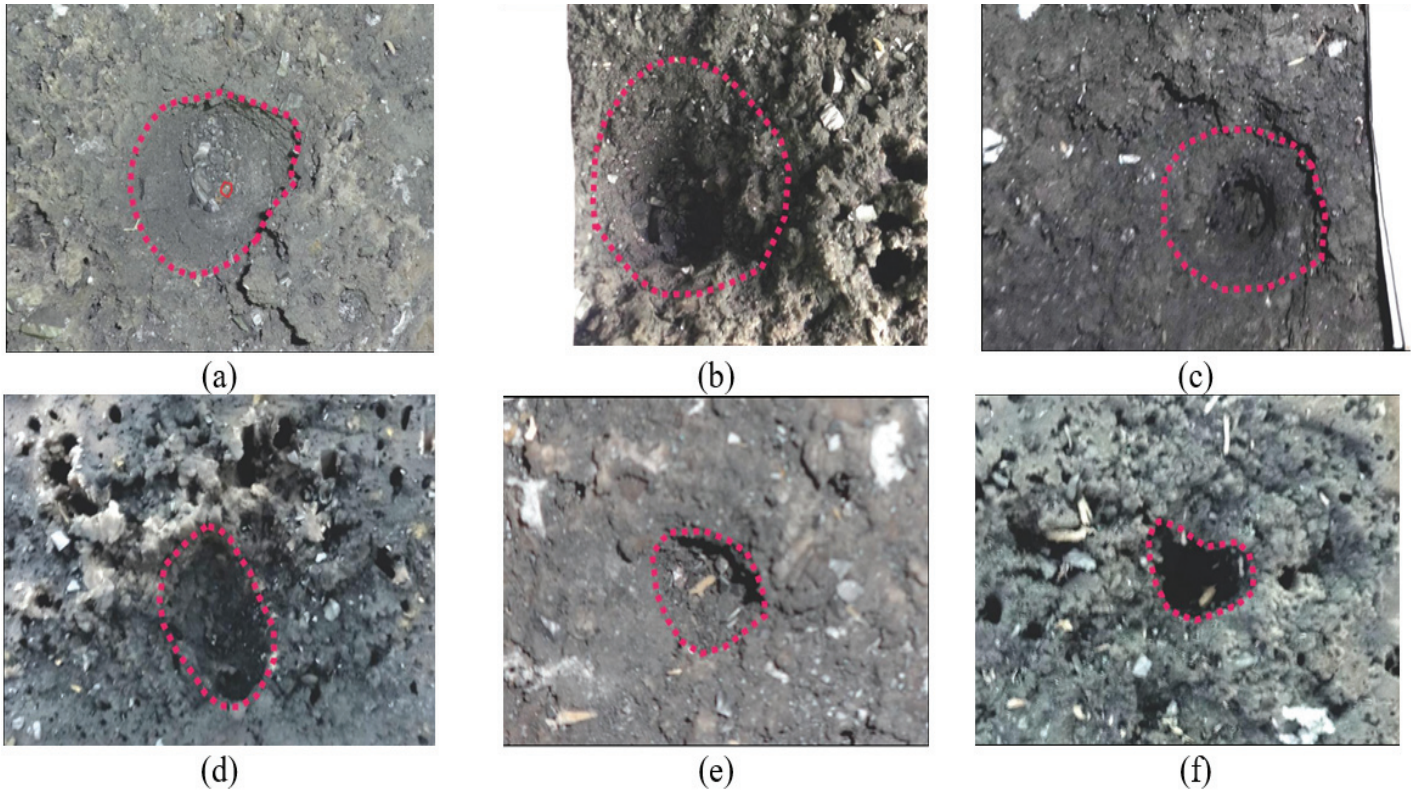

Figure 5. Crater diameter generated by WC-8Co (a-c) and steel (Pindad standard) (d-f) as the front core of the projectile on the backing target (plasticine clay).

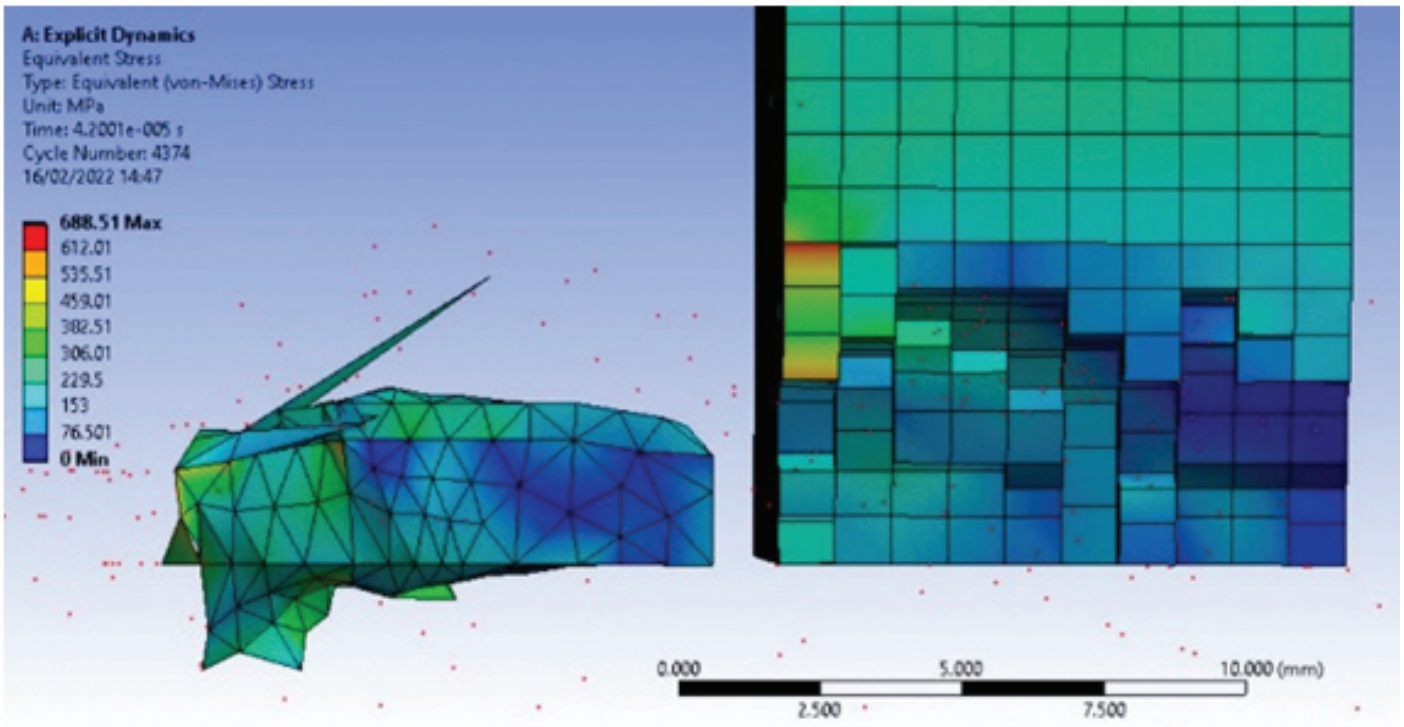

(a)

Figure 6. Equivalent (Von-Mises) stress and strain for steel (Pindad standard) (a-b) and WC-8Co (c-d) as the front core of the projectile.

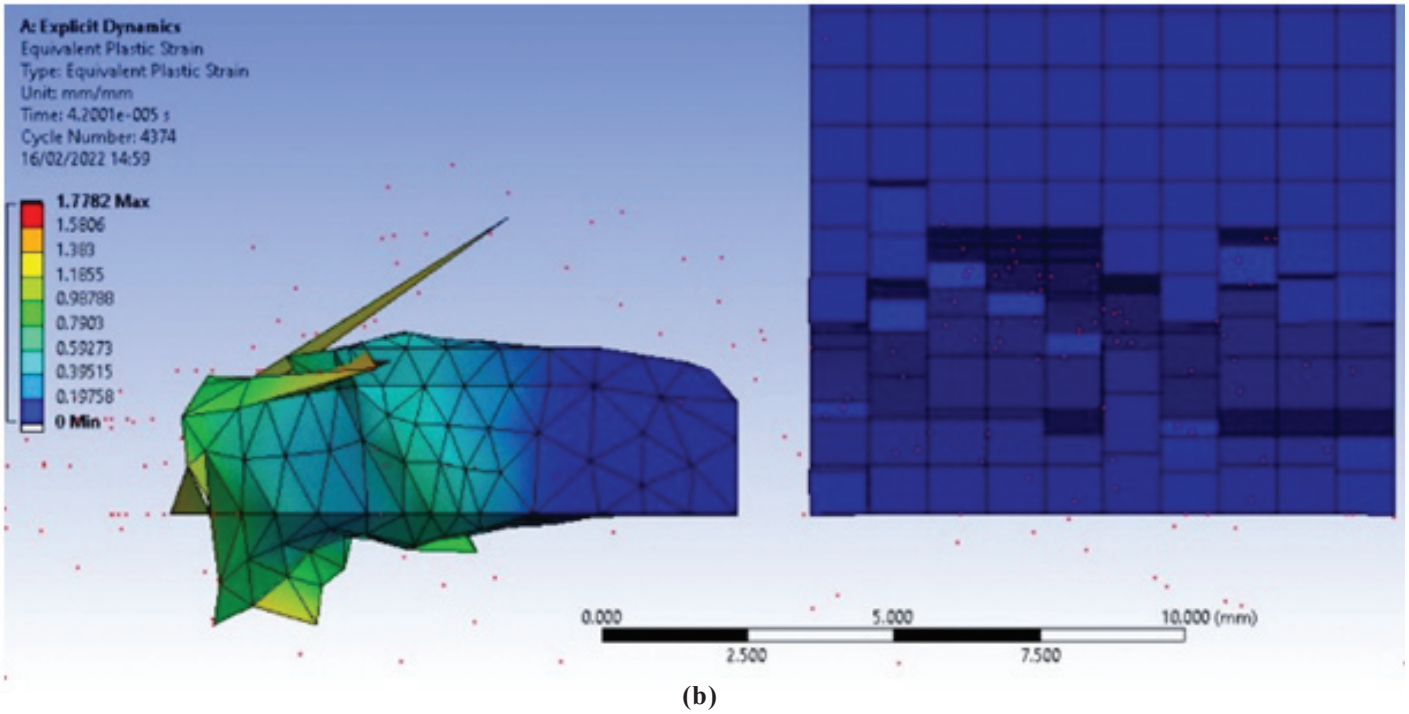

(b)

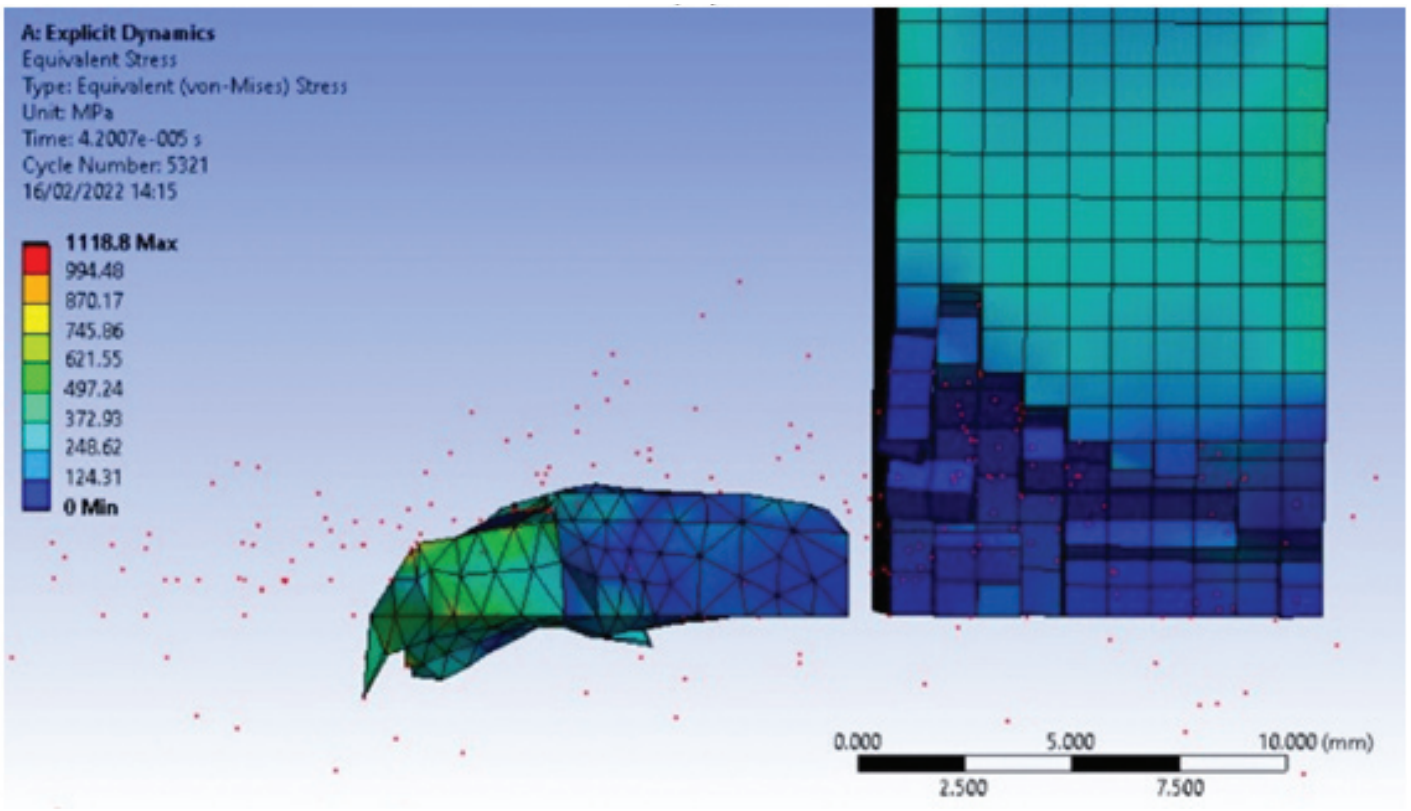

(c)

Figure 6. Equivalent (Von-Mises) stress and strain for steel (Pindad standard) (a-b) and WC-8Co (c-d) as the front core of the projectile.

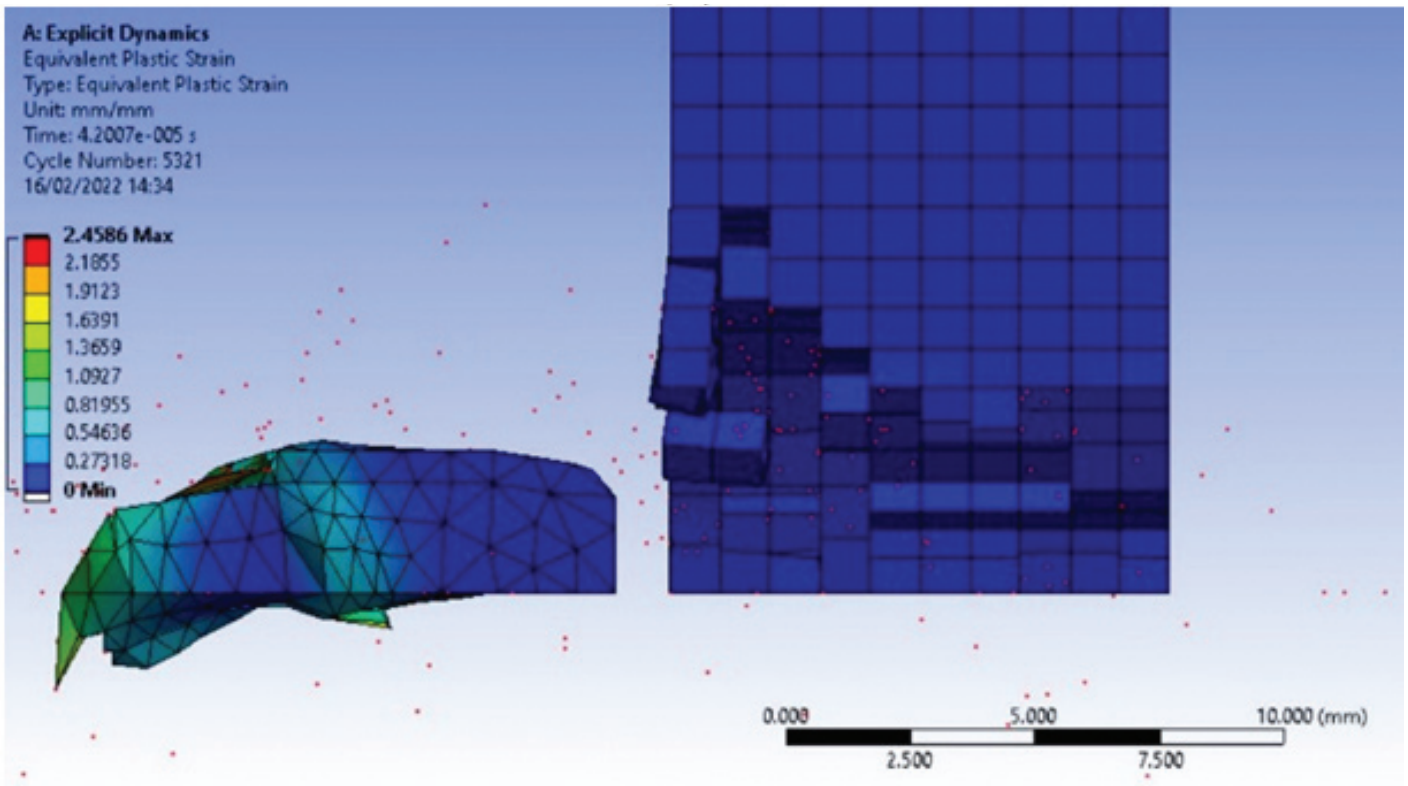

(d)

Figure 6. Equivalent (Von-Mises) stress and strain for steel (Pindad standard) (a-b) and WC-8Co (c-d) as the front core of the projectile.

4. CONCLUSION

In summary, our study has demonstrated that the projectile using WC-8Co for its front core in terms of 5.56 × 45 mm calibre ammunition showed greater performance in penetrating the SiC target compared to the steel (Pindad standard) core projectile. This projectile also was capable of respectively generating 1.5 and 1.8 times greater DoP and craters than the projectile with front core of steel (Pindad standard). Additionally, the projectile with WC-8Co as its front core also produced 1.3 times higher residual velocity than the steel (Pindad standard) core projectile. The kinetic energy impact of the projectile had a linear correlation with DoP and residual velocity, while the hardness of the projectile core exhibited an inverse relation with the volume of the residual projectile. The greater the hardness of the projectile, therefore, the lower the volume of the residual projectile residual and the bigger the crater generated. These findings indicate the potential development of WC-8Co as front bullet core material to improve the penetration of projectiles into ceramic armour.

ACKNOWLEDGEMENTS

The authors thank the Indonesia Defense University (IDU), PT. Pindad (Persero), and the Research Center for Physics & Directorate of Repositories, Multimedia, and Scientific Publishing Affairs – National Research and Innovation Agency for providing the materials and facilitating the equipment and software for the research. In addition, we would also like to thank Mr. Djatmiko Erlambang, S.T from PT. OPTIMAXX Prima Teknik (OPT) for his help and suggestions in relation to the numerical simulation process.

REFERENCES

1. National Research Council of the National Academies. Testing of Body Armor Materials: Phase III. The National Academic Press, US, 2012. 340. doi:10.17226/13390
2. Yi, R.; Yin, L.; Wang, J.; Chen, Zhi-gang & Hu, Di-qi. Study on the performance of ceramic composite projectile penetrating into ceramic composite target. *Def. Technol. J.*, 2017, **13**(4), 295-299. doi: 10.1016/j.dt.2017.05.009.
3. Skaggs, S.R. A brief history of ceramic armor development. *In* Proceeding of 27th Annual Cocoa Beach Conference on Advanced Ceramics and Composites: A: Ceramic Engineering and Science, 2003, **24**(3). doi: 10.1002/9780470294802.ch51
4. Basyir, A.; Agustian, E.S. & Amelia, A. A review of penetraton of tungsten based projectile on depth of penetration at armor of ceramic based. *Jurnal Pertahanan*,

2020, **6**(3), 286-309.
doi: 10.33172/jp.v6i3.890

5. Kaufmann, C.; Cronin, D.; Worswick, M.; Pageau, Gilles & Beth, Andre. Influence of material properties on the ballistic performance of ceramics for personal body armour. *Shock Vib.*, 2003, **10**(1), 51-58.
doi: 10.1155/2003/357637
6. Arslan, G. & Kalemtas, A. Processing of silicon carbide-boron carbide-aluminium composites. *J. Eu. Ceramic Soc.*, 2009, **29**(3), 473-480.
doi: 10.1016/j.jeurceramsoc.2008.06.007
7. Holmquist, T. J.; Johnson, G.R. & Gooch, W.A. Modeling the 14.5 mm BS41 projectile for ballistic impact computations. *In* Computational Ballistics II, edited by V. Sanchez-Galvez, C. A. Brebbia, A. A. Motta, & C. E. Anderson. WIT Press, Southampton, England, UK, 2005. Pp. 61-75.
8. Lundberg, P. & Lundberg, B. Transition between interface defeat and penetration for tungsten projectiles and four silicon carbide materials. *Int. J. Impact Engin.*, 2005, **31**(7), 781-792.
doi: 10.1016/j.ijimpeng.2004.06.003.
9. Behner, T.; Heine, A. & Wickert, M. Dwell and penetration of tungsten heavy alloy long-rod penetrators impacting unconfined finite-thickness silicon carbide ceramic targets. *Int. J. Impact Engin.*, 2016, **95**, 54-60.
doi: 10.1016/j.ijimpeng.2016.04.008.
10. Luo, D.; Wang, Y.; Wang, F.; Cheng, H.; Zhang, Bowen & Zhu, Yu. The influence of metal cover plates on ballistic performance of silicon carbide subjected to large-scale tungsten projectile. *Mater. Des*. 2020, **191**(108659), 1-12.
doi: 10.1016/j.matdes.2020.108659
11. Yuan, J.; Tan, G.E.B. & Goh, W.L. Simulation of dwell-to-penetration transition for SiC ceramics subjected to impact of tungsten long rods. *In* Proceedings of the 14th Armor Ceramics Symposium – 40th International Conference on Advanced Ceramics and Composites 2017.
doi: 10.1002/9781119321682.ch8
12. Shoufa, L. Oxidation behavior of WC–Co cemented carbide in elevated temperature. *Mater. Res. Express*. 2018, **5**(9), 095801.
doi:10.1088/2053-1591/aad535
13. Siwak, P. & Garbiec, D. Microstructure and mechanical properties of WC–Co, WC–Co–Cr_3C_2 and WC–Co–TaC cermets fabricated by spark plasma sintering. *Transact. Nonferrous Met. Soc. China*. 2016, **26**(10), 2641-2646.
doi: 10.1016/S1003-6326(16)64390-X
14. Aristizabal, M.; Sanchez, J.M.; Rodriguez, N.; Ibarreta, Federico & Martinez, Roberto. Comparison of the oxidation behaviour of WC–Co and WC–Ni–Co–Cr cemented carbides. *Corros. Sci*. 2011, **53**(9), 2754-2760.
doi: 10.1016/j.corsci.2011.05.006
15. Arora, A. & Rao, V.G. Tungsten heavy alloy for defence applications. *Mater. Technol*. 2004, **19**(4), 210-215.
doi: 10.1080/10667857.2004.11753087
16. Hamidi, A.G.; Arabi, H. & Khaki, J.V. Sintering of a nano crystalline tungsten heavy alloy powder. *Int. J. Refract. Met. Hard Mater.*. 2019, **80**, 204-209.
doi: 10.1016/j.ijrmhm.2019.01.016
17. Qiang, L.X.; Wei, X.H.; Ke, Hu & Li, Yuan-yuan. Microstructure and properties of ultra-fine tungsten heavy alloys prepared by mechanical alloying and electric current activated sintering. *Transact. Nonferrous Met. Soc. China*. 2010, **20**(3), 443-449.
doi: 10.1016/S1003-6326(09)60160-6
18. Chen, C. L. & Ma, S.H. Study on characteristics and sintering behavior of W-Ni-Co tungsten heavy alloy by a secondary ball milling method. *J. Alloys Compd*. 2018, **731**, 78-83.
doi: 10.1016/j.jallcom.2017.09.125
19. Chen, C. L. & Ma, S.H. Study on combination of in-situ dispersion and secondary ball milling for W-Ni-Co tungsten heavy alloy. *Int. J. Refract. Met. . Hard Mater*. 2018, **71**, 8-14.
doi: 10.1016/j.ijrmhm.2017.10.010
20. Senthilnathan, N.; Annamalai, A.R. & Venkatachalam, G. Microstructure and mechanical properties of spark plasma sintered tungsten heavy alloys. *Mater. Sci. Engin.: A*. 2018, **710**, 66-73.
doi: 10.1016/j.msea.2017.10.080
21. Klapotke, T.M. Reactive structure materials. *Engin. Sci. Mil. Technol*. 2020, **4**(2), 171-177.
doi: 10.21608/EJMTC.2021.72401.1183
22. Evers, J.; Huber, S.; Oehlinger, Gilbert & Klapotke, Thomas M. Properties in reactive structure materials: ZrW_2 and HfW_2 - high melting temperatures, densities, hardness and exothermic ignition energies. *J. Inorg. Gen. Chem*. 2020, **646**(22), 1805-1811.
doi: 10.1002/zaac.202000237
23. Deligoz, E.; Ozisik, H. & Colakoglu, K. Theoretical predictions of the structural, mechanical and lattice dynamical properties of XW_2 (X = Zr, Hf) Laves phases. *Philos. Mag*. 2014, **94**(13), 1379-1392.
doi: 10.1080/14786435.2014.886024
24. Basyir, A.; Bura, R.O. & Lesmana, D. Experimental consideration of projectile density and hardness effect on its penetration ability in alumina target. *J. Def. Acqui. Technol.*, 2019, **1**(1), 9–15.
doi: 10.33530/jdaat.2019.1.1.9
25. Ding, X.Y.; Luo, L.M.; Huang, L.M.; Luo, G.N.; Zhu, X.Y.; Cheng, Ji-Gui & Wu, Yu-Cheng. Preparation of TiC/W core–shell structured powders by one-step activation and chemical reduction process. *J. Alloys Compd*. 2015, **619**, 704-708.
doi: 10.1016/j.jallcom.2014.08.242
26. Liu, K.; Wang, Z.; Yin, Z.; Cao, Liyan & Yuan, Juntang. Effect of Co content on microstructure and mechanical properties of ultrafine grained WC-Co cemented carbide sintered by spark plasma sintering, *Cera. Int.*, 2018, **44**(15), 18711-18718.
doi: 10.1016/j.ceramint.2018.07.100
27. Klunsner, T.; Marsoner, S.; Ebner, R.; Pippan, R.; Glatzle, Johannes & Puschel, Arndt. Effect of microstructure on fatigue properties of WC-Co hard metals. *Procedia Eng*.

2010, **2**, 2001-2010.
doi: 10.1016/j.proeng.2010.03.215.
28. Saito, H.; Iwabuchi, Akira & Shimizu, Tomoharu. Effects of Co content and WC grain size on wear of WC cemented carbide. *Wear*. 2006, **261**, 126-132.
doi: 10.1016/j.wear.2005.09.034.
29. NATO Standardization Office. Document of Standardization agreement of bullet impact munition test procedures-Edition 3. STANAG 4241:2018, Brussels, Belgium. STANAG, 2018.
30. Mukasey, M.B.; Sedgwick, J.L. & Hagy, D.W. Document of National Institute of Justice Standard of ballistic resistance of body armor. NIJ Standard-0101.06:2008, Washington, US, NIJ, 2008. URL: https://www.ojp.gov/pdffiles1/nij/223054.pdf
31. Medvedovski, E. Ballistic performance of armour ceramics: influence of design and structure Part 2. *Ceram. Int.*, 2010, **36**(7), 2117–2127.
doi: 10.1016/j.ceramint.2010.05.022.
32. Crouch, Ian G. The science of armour materials. Woodhead Publishing Material, England, UK, 2017. 715 p.
33. NATO Standardization Office. Document of Standardization agreement of 5.56 ammunition-Edition 2. STANAG 4172:1993, Brussels, Belgium. STANAG, 1993.
34. Rohr, I.; Nahme, H.; Thoma, Klaus & Anderson, Charles E. Material characterisation and constitutive modelling of a tungsten-sintered alloy for a wide range of strain rates. *Int. J. Impact Engin*. 2008, **35**(8), 811–819.
doi: 10.1016/j.ijimpeng.2007.12.006.
35. Johnson, G.R. & Cook, W.H. Fracture characteristics of three metals subjected to various strains, strain rates, temperatures and pressures. *Engin. Fract. Mech.*, 1985, **21**(1): 31–48.
doi: 10.1016/0013-7944(85)90052-9.
36. Flores-Johnson, E. A.; Saleh, M. & Edwards. L. Ballistic performance of multi-layered metallic plates impacted by a 7.62-mm APM2 projectile. *Int. J. Impact Eng*. 2011, **38**(12), 1022–1032.
doi: 10.1016/j.ijimpeng.2011.08.005.
37. Woolmore, N.J. The failure of a tungsten carbide – cobalt cored projectil penetrating a hard target. Cranfield University, Cranfield, UK, 2005. (PhD Thesis).
38. Husain, A.; Ansari, R. & Khan, Arshad H. Experimental and numerical investigation of perforation of thin polycarbonate plate by projectiles of different nose shape. *Latin Am. J. Solids Struct.*. 2016, **4**, 357-372.
doi: 10.1590/1679-78253252.
39. Peng, Y.; Wu, H.; Fang, Qin & Gong, Ziming. Deceleration time of projectile penetration/perforation into a concrete target: experiment and discussions. *Adv. Struct. Eng*. 2019, **22**(1), 112-125. doi: 10.1177/1369433218779235
40. Prasob, P.A.; Sasikumar, M.; Bardiya, Navneet & Vasundhra, P. Projectile penetrating multilayer composite armor. *Indian J. Sci. Technol.*, 2016, **9**(47), 1-7.
doi: 10.17485/ijst/2016/v9i47/107923
41. Igelegbai, E.E.; Alo, O.A.; Adeodu, Adefemi O. & Daniyan, Ilesanmi A. Evaluation of mechanical and microstructural properties of α-brass alloy produced from scrap copper and zinc metal through sand casting process. *J. Miner. Mater. Charact. Eng*. 2017, **5**(1), 18–28.
doi: 10.4236/jmmce.2017.51002
42. Crouch, Ian G. Body armour – new materials, new system. *Def. Technol*. 2019, **15**(3), 241-253.
doi: 10.1016/j.dt.2019.02.002.
43. Bracamonte, L.; Loutfy, R.; Yilmazcoban, Ibrahim K. & Rajan, Subrarnaniam D. Design, manufacture, and analysis of ceramic-composite armor. *In* Lightweight ballistic composites: Military and law-enforcement applications, 2nd Edition. Woodhead Publishing Series in Composites Science and Engineering, Cambridge, England, UK, 2016. pp. 349–367.
doi: 10.1016/B978-0-08-100406-7.00012-X.

CONTRIBUTORS

Mr Abdul Basyir received his Master of Defense in the Weaponry Technology Department from Indonesia Defense University. He worked as a researcher in the High Resistant Material Research Group, Research Center for Physics, National Research and Innovation Agency since 2021. His research interests are terminal ballistics, synthesis and characterisation of tracer projectile composition and oxidation resistance material, metal powderisation by gas atomisation method, and characterisation of shale hydrocarbon potential based on advance processing and log data.
He created the research idea, wrote the original paper, performed experimental and numerical simulation, and investigated finding of this research.

Dr Romie Oktovianus Bura obtained PhD from Aerospace Engineering major in University of Southampton, UK. He is the lecturer of the Faculty of Defense Technology, Indonesia Defense University. His research interest is high-speed aerodynamic, design and propulsion; shock-related fluid dynamics and hypersonic flow as well as airframe-propulsion integration.
He supervised and reviewed original paper and verified numerical simulation method.

Mr Denny Lesmana received his MSc degrees (Defence and Security) at Cranfield University, the UK in 2018. He worked as an expert of ammunition development in PT. Pindad (Persero), Turen, Indonesia. His research interests are ammunition design, warhead system, engineering simulation (CFD & Structural Analysis), fragmentation, and defeat mechanism.
He reviewed original paper, supervised experimental and numerical analysis, and designed ballistic test.

Ms Lucia Dwi Antika obtained her Master Degree in Food Science and Nutrition, Hallym University, South Korea. She is conducting molecular nutritional research work. She is working as a researcher in the Research Center for Chemistry, Indonesian Institute of Sciences from 2019 to 2021 and National Research and Innovation Agency since 2021.
She edited and reviewed original paper and involved in original paper writing.